Available online at www.sciencedirect.com

ScienceDirect

Journal of the European Ceramic Society 35 (2015) 723–730

www.elsevier.com/locate/jeurceramsoc

Preparation and characterization of hydrophobic alumina planar membranes for water desalination

Chunlei Ren [a], Hong Fang [a], Jianqiang Gu [a], Louis Winnubst [a,b], Chusheng Chen [a,*]

[a] *CAS Key Laboratory of Advanced Materials for Energy Conversion and Department of Materials Science and Engineering, University of Science and Technology of China, Hefei, Anhui 230026, PR China*

[b] *Inorganic Membranes, MESA+ Institute for Nanotechnology, University of Twente, P.O. Box 217, 7500 AE Enschede, The Netherlands*

Received 25 April 2014; received in revised form 4 July 2014; accepted 8 July 2014
Available online 3 October 2014

Abstract

A planar alumina membrane was prepared by a one-step phase-inversion tape casting method. The membrane consisted of a thick support layer with finger-like large pores and a thin separation layer containing small pores with an average diameter of ~0.76 μm. The overall porosity of the membrane was ~59%, as determined with the Archimedes method, and the porosity associated with the large, finger-like pores in the support layer was ~34% as derived from image analysis. The surface of this alumina membrane was converted from hydrophilic to hydrophobic via grafting with a fluoroalkylsilane. The water desalination performance was tested by exposing the hydrophobic separation layer to an aqueous solution of 2 wt.% NaCl at 80 °C, while a sweep of distilled water at 20 °C was used, resulting in a water flux of 19.1 L m^{-2} h^{-1} and a salt rejection over 99.5%. Due to the excellent water desalination performance, the hydrophobic porous ceramic membrane holds promise for practical applications.

Keywords: Phase-inversion tape casting; Alumina; Surface grafting; Hydrophobicity; Membrane distillation

1. Introduction

In view of the global shortage of clean water, it is highly recommended to develop new methods for water treatment.[1,2] Compared with conventional separation processes like reverse osmosis or thermal evaporation, membrane distillation (MD) is expected to be a cost-effective technology for seawater desalination, due to low demands on heat source and operating pressure. Hydrophobic materials, such as polypropylene (PP), polytetrafluoroethylene (PTFE), polyvinylidenefluoride (PVDF), are widely used as MD material.[3] In comparison with polymers, hydrophobic ceramic membranes are much more desirable owing to their better chemical and thermal stability. Most ceramic membranes are naturally hydrophilic because of the surface hydroxyl. Therefore, they have to be modified with low surface energy materials before used for MD. The first work on hydrophobic ceramic membranes for membrane distillation was reported by Larbot in 2004.[4] Since then, a few ceramic membranes have been successfully prepared and applied in MD for water desalination, resulting in salt rejections of more than 95%.[5–7] However, MD also has some drawbacks such as low flux and high susceptibility to variation of salt concentration and feed temperature.[8] In general hydrophobic ceramic membranes with large flux, excellent salt rejection, sufficient mechanical strength and chemical stability are required for MD application.[9]

It is well known that mass transfer through a membrane largely depends on its thickness, porosity and pore size distribution.[10] It is desired to use a porous ceramic membrane with small transport resistance. Typically, a porous ceramic membrane consists of a multi-layered asymmetric structure: one or more thin top layers with small pores, enabling separation, and a thick bulk layer with large pores providing mechanical strength.[11,12] Very often the fabrication of such an asymmetric structure involves multiple steps. A support layer is first prepared, followed by coating an intermediate layer and application

* Corresponding author. Tel.: +86 551 63600088; fax: +86 551 63631760.
E-mail address: ccsm@ustc.edu.cn (C. Chen).

http://dx.doi.org/10.1016/j.jeurceramsoc.2014.07.012
0955-2219/

of the final separation layer. Each step involves high temperature sintering, making the ceramic membrane fabrication expensive. Clearly, combining the multiple steps into a single one is desirable in reducing production time and costs.

Recently, it is reported that ceramic membranes with the as-above described asymmetric structure can be prepared conveniently by phase-inversion tape casting.[13,14] Here a slurry of a ceramic powder in an organic polymer solution is cast on a temporary substrate, and then immersed into a water bath in which the organic polymer solution separates into a polymer-rich phase and a polymer-lean phase as a result of exchange of organic solvent with water. The slurry is solidified into a green tape due to the occurrence of the polymer-rich phase, and large finger-like pores are created in the green tape after removal of the polymer-lean phase. Since the phase-inversion process initiates from the slurry–water interface and proceeds into the bulk, the as-formed green tape possesses a two-layered structure: a thick layer containing finger-like large pores over a thin layer free of large pores. This asymmetric two-layered structure is preserved after firing of the green tape at elevated temperatures.

In the present study, porous alumina with asymmetric two-layered structure was formed using the phase-inversion tape casting method, and the surface of the alumina was further modified with a hydrophobic fluoroalkylsilane (FAS). The gas/liquid permeation as well as MD desalination properties of the as-prepared membrane was studied.

2. Experimental

2.1. Fabrication of alumina planar membranes

Phase inversion-tape casting method was used to fabricate the membranes. Details can be found elsewhere.[14] Briefly, polyethersulfone (6.2 wt.%) (PES) (Gafone 3000, Solvay Advanced Polymers) and polyvinylpyrrolidone (0.9 wt.%) (PVP) (K30, CP, Sinopharm Chemical Reagent Co.) were dissolved in N-methyl-2-pyrrolidone (31.0 wt.%) (NMP) (CP, Sinopharm Chemical Reagent Co., China) to form a stable polymer solution. Subsequently α-Al_2O_3 powder (61.9 wt.%) with an average particle size of 0.8 μm (Zhenghai, Jiangsu, China) was added to the solution. This mixture was mixed/milled for 48 h at room temperature, using a planetary mill. The as-prepared slurry was degassed for 10 min using a vacuum pump (2XZ-2, Tanshi, Linhai, China), and then casted on a Mylar sheet with a doctor blade of gap height 1.0 mm and motion speed 20 cm/min. The casted slurry was immediately immersed in water at room temperature and left for 24 h for coagulation. After drying under ambient conditions, the green tape was cut into round pieces with a diameter of 40 mm, then heated at a rate of 2 °C/min to 800 °C and kept at this temperature for 4 h to remove the polymer binder, followed by heating to 1500 °C at a rate of 2 °C/min and being held for 10 h. The samples were cooled down to room temperature at a rate of 2 °C/min. The whole sintering procedure was processed in air.

2.2. Surface grafting with fluoroalkylsilanes

Prior to surface grafting, the sintered alumina wafers were ultrasonically cleaned respectively in acetone, ethanol and water for 10 min. The wafers were dried at 100 °C for 2 h, immersed into a 2 wt.% FAS (1H,1H,2H,2H-perfluorooctyltriethoxysilane, DYNASYLAN, F8261) in ethanol solution at room temperature and left in this solution for 24 h to allow the coupling reaction to occur. After immersion the wafers were dried at 100 °C for 6 h. The immersion and drying processes were repeated three times. Finally, the membranes were stored at room temperature and ready for water desalination experiments.

2.3. Characterization

The dried green tape was analyzed using TGA and DSC (DTG-60H, Shimadzu). A sample was heated from room temperature to 1400 °C at a rate of 5 °C/min in air. Densification of the green body was analyzed by a dilatometer (DIL 402 C, Netzsch). A strip of green tape with a length of 9 mm a width of 3 mm and a thickness of 0.78 mm was heated to 1500 °C at a rate of 5 °C/min, the contraction along the length direction was measured with the increase of temperature.

The morphology of green tape and ceramic wafer was observed with scanning electron microscopy (SEM; JSM-6700F, JEOL, Japan) at an accelerating voltage of 20 kV. Prior to SEM observations the samples were covered with gold by means of sputtering.

The density of the ceramic wafer, ρ, was measured using the Archimedes method in mercury. The porosity was calculated using the formula $(1 - \rho/\rho_{th}) \times 100\%$ where ρ_{th} is the theoretical density of α-alumina. The porosity was also determined from images taken from back-scattered electron (BSE) mode of the SEM, using the Otsu's method as described elsewhere.[15] Otsu's method is a threshold selection method from gray-level histograms to distinguish different phases in an image. A better contrast between solid and pore can be obtained by using BSE image compared with secondary electron images. Finally the pore size distribution of the ceramic wafer was measured by the bubble point method.[16]

Nitrogen gas and pure water flux through ceramic wafers with a diameter of 20 mm were analyzed using a home-made equipment. A sample was fixed on a male connector, and then covered by a refined cylinder. Nitrogen was fed into the cylinder at various pressures, and the amount of permeated N_2 was measured with a soap bubble flow meter. Similarly, pure water permeation tests were performed and the weight of the permeated water was measured by an electronic balance.

The water contact angles of the membranes before and after grafting were measured using a contact angle meter (SL200B, Chenghui, China). The volume of a deionized water droplet was ~5 μL, and the average value of five measurements, performed at different positions on the same sample, was adopted as the contact angle.

Direct contact membrane distillation (DCMD) experiments were conducted using a home-made MD set-up, as shown in

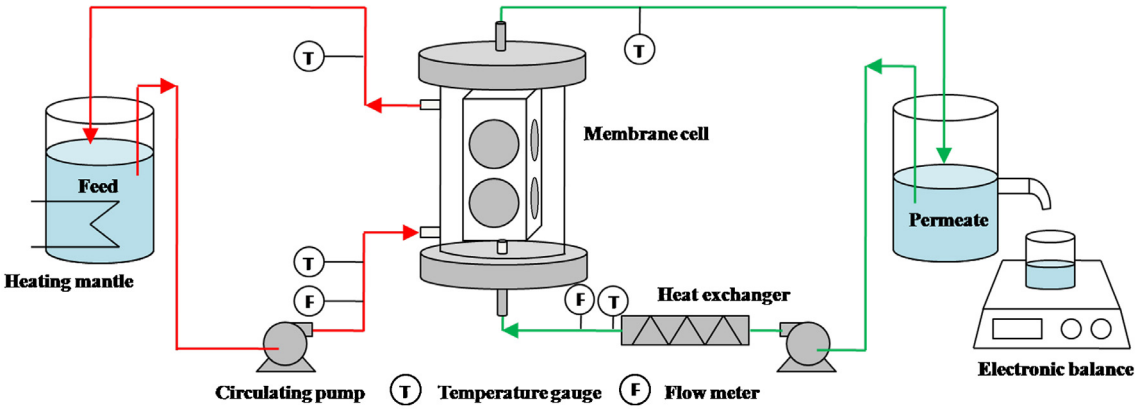

Fig. 1. Schematic diagram of the experimental DCMD set-up.

Fig. 1. The planar membrane module consisted of 8 wafers (on four sides of the cube in Fig. 1), each with a diameter of 32 mm, the total membrane surface area was 64.3 cm^2. Aqueous solutions of NaCl with different concentrations (2, 4, 6 wt.%) were used as feed, heated by a heating mantle to fixed temperatures of 50, 60, 70 and 80 °C. The NaCl solution was circulated at a flow rate of 0.03 m/s by using a circulating pump. At the permeate side of the membranes distilled water was used as sweep at the same fluid velocity of 0.03 m/s and a fixed temperature of 20 ± 2 °C (using a thermostatic bath). The water flux through the membranes was quantified by measuring the mass using an electronic balance, and a conductivity meter (FE30, Mettler Toledo) was used to measure the conductivities of the feed and permeate water, salt rejection (R) was calculated by the following equation.[17]

$$R = \left(1 - \frac{C_p}{C_f}\right) \times 100\% \quad (1)$$

where C_p and C_f are the conductivities of the feed and permeate water. In the DCMD mode, the permeate water vapor is directly condensed on the cooling flow and the conductivity of cold stream was used as approximate value of C_p. The conductivity of the cold stream was also monitored with time.

3. Results and discussion

3.1. Sintering behavior of the green tape

Fig. 2 shows the TGA/DSC curves of the dried green tape in air. A gradual weight loss occurred with increasing temperature from room temperature to ~500 °C, which was related to the removal of the residual solvent and sluggish oxidation of the polymers in the green tape. A drastic weight loss and a strong exothermic peak appeared in the temperature range from ~500 to ~600 °C, which was associated to burning-out of the polymers. Further increase in temperature did not lead to any further noticeable weight loss. The total weight loss of ~10% was equal to the weight fraction of the polymers (PES and PVP) in the dried green tape, indicating the complete removal of the polymers.

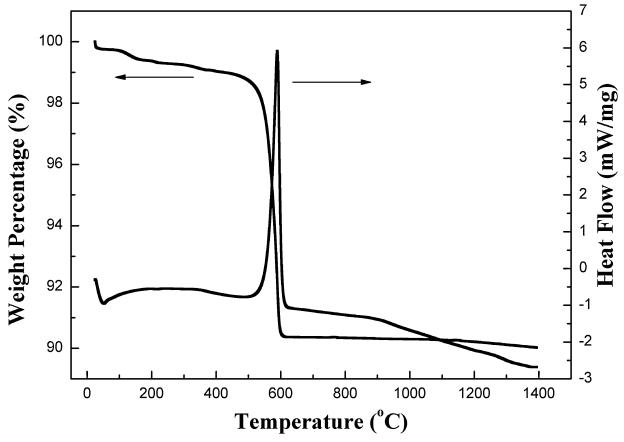

Fig. 2. TGA and DSC curves of a green tape with a heating rate of 5 °C/min in air.

Fig. 3 shows the linear shrinkage of a green tape at a constant heating rate of 5 °C/min. A linear shrinkage of around 1% occurred in the temperature range of 200–300 °C, corresponding to the viscous deformation of the contained polymers.[18] A small, but noticeable shrinkage appeared at a temperature of ~500 °C, which was attributed to burning-out of the polymers. Large shrinkage appeared at temperatures above ~1100 °C, which was

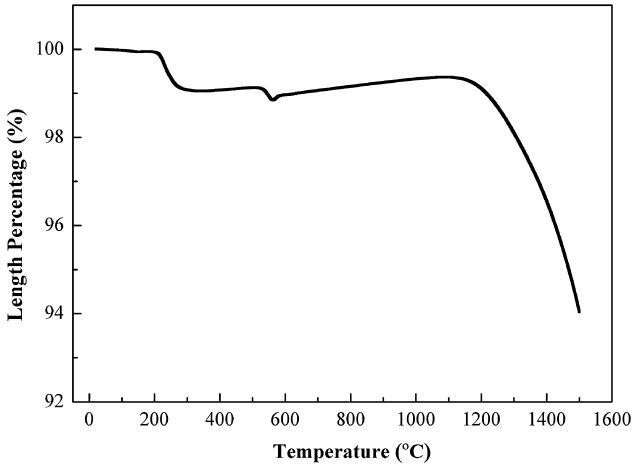

Fig. 3. Linear shrinkage of a green tape with a heating rate of 5 °C/min in air.

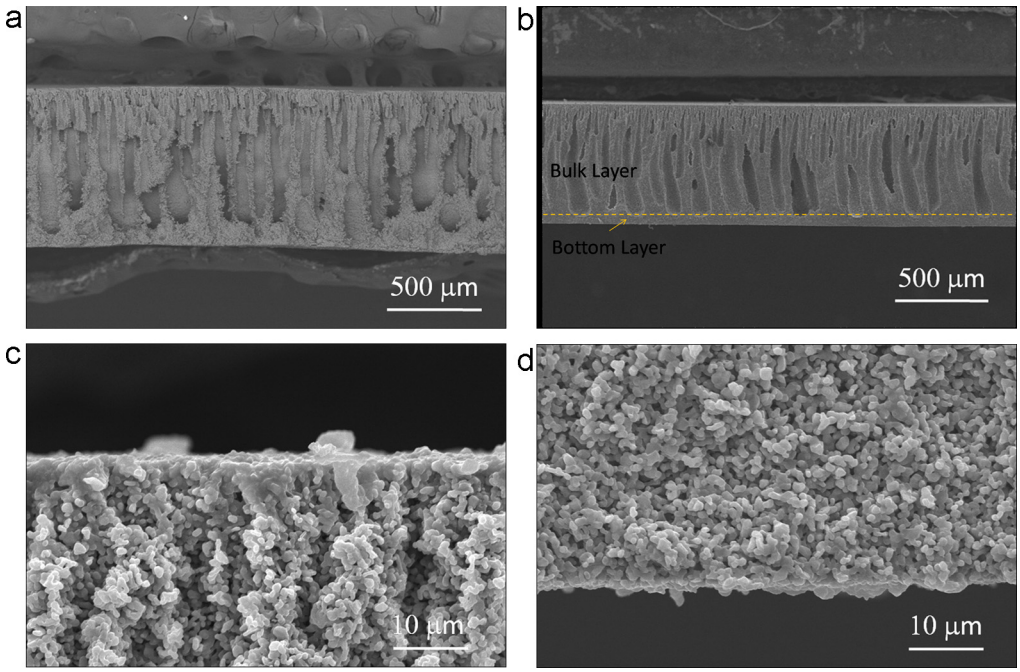

Fig. 4. SEM images of cross sections of (A) a green tape, (B) a sintered ceramic wafer, (C) near the top surface after sintering, (D) near the bottom surface after sintering.

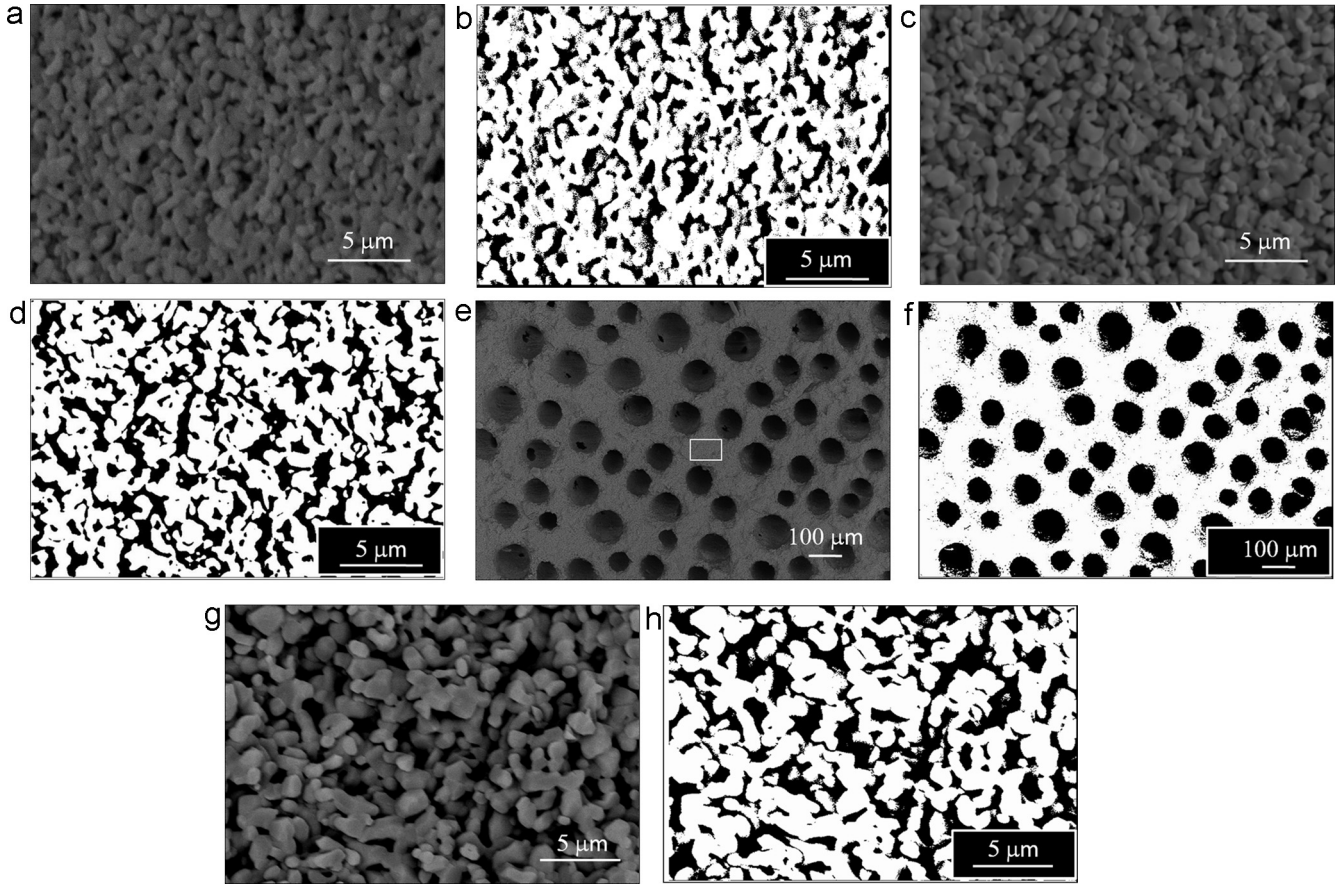

Fig. 5. BSE-SEM and threshold images of a ceramic wafer. (A and B) Top surface; (C and D) bottom surface; (E and F) bulk; (G and H) the close-up image of the wall of macro-voids shown in (E).

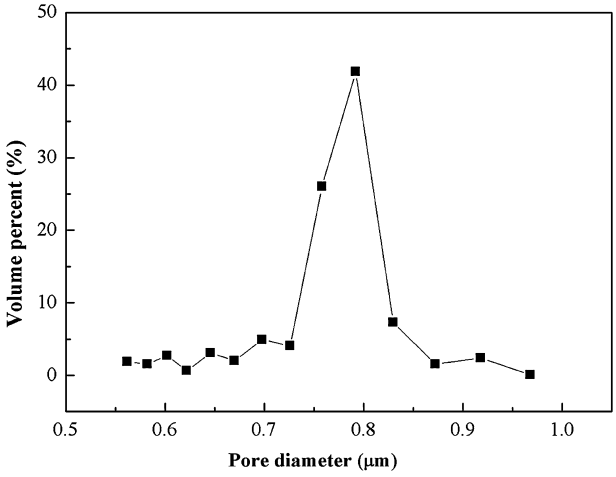

Fig. 6. Testing results of pore size distribution of a ceramic wafer with the bubble-point method.

related to densification of alumina. A total linear shrinkage of 6% was attained when the sample was heated to a temperature of 1500 °C.

3.2. Morphology

Fig. 4A and B show cross-sectional SEM images of a green and sintered tape, respectively. The green tape contained elongated finger-like large pores (Fig. 4A) which are often found in materials formed by the phase inversion method.[19] Those macrovoids were still present after sintering (Fig. 4B). The close-up images of the top layer revealed that the macrovoids were initiated from the top surface where the initial exchange of solvent in the ceramic/polymer slurry with non-solvent in the coagulation bath took place (Fig. 4C). The macrovoids penetrated into the bulk, but did not reach the bottom layer (Fig. 4D).

Fig. 5 presents SEM cross-section images (perpendicular to the thickness direction) of the ceramic wafer. The SEM images were taken in the back-scattered electron (BSE) emission mode. Since the solid phase and the pore showed a large difference in intensity of the BSE signal, these phases can be discriminated by converting the grayscale images into binary ones using Otsu's threshold method.[20] In the as-obtained binary images (Fig. 5B, D, F and H), the black and white regions corresponded to pore space and solid phase, respectively. It can clearly be seen that both the top and bottom surfaces of the wafer contained micrometer-sized pores (Fig. 5A–D). The bulk of the wafer contained macrovoids of a few ten micrometers in diameter (Fig. 5E and F), while a close-up view of the wall of the macro-voids revealed the presence of micrometer-sized pores (Fig. 5G and H).

Fig. 6 presents the results of pore size distribution measured by the bubble-point method. It can be seen that the membrane exhibited a homogeneous pore size distribution. The diameter of most pores (~84%) was in the range of 0.70–0.87 μm and the average pore size was about 0.76 μm. According to the principle of this method, this value corresponds to the narrowest position of through-pores, i.e., the pore-throat.[21] Based on the

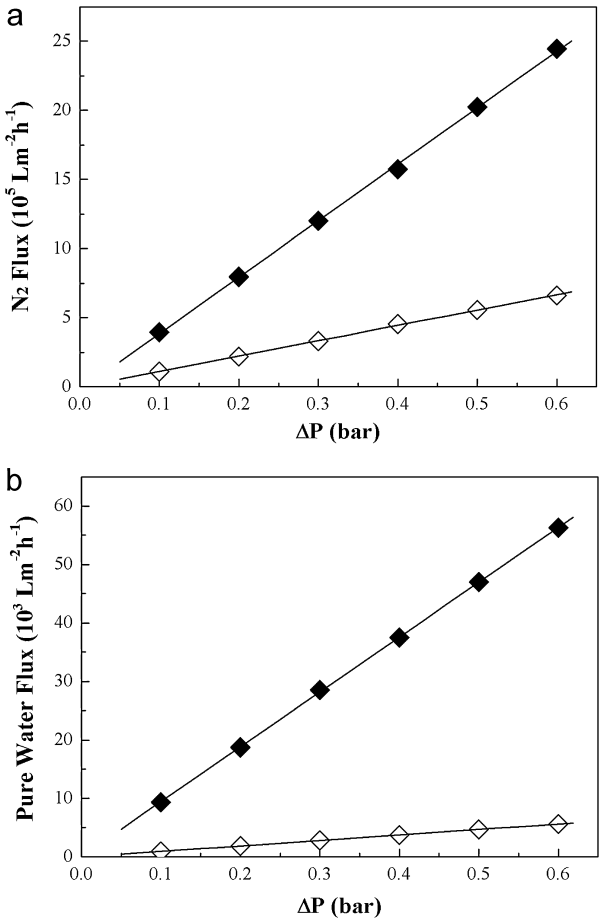

Fig. 7. (A) N_2 and (B) pure water flux of a ceramic wafer. The open and filled symbols correspond to the ceramic wafer before and after removal of the bottom layer, respectively.

observation on the cross-sectional image (Fig. 4D), the pore-throat was believed to lie in the near-bottom region of the wafer, in which region macrovoids were absent whereas the small pores were still present.

3.3. Porosity

The porosity of the whole ceramic wafer was determined to be ~59% by using the Archimedes method in mercury. The porosity was also determined from SEM-BSE binary images of the wafer by calculating the percentage of pixels assigned to the pores.[15] For the top and bottom surfaces (Fig. 5B and D), the porosities were ~31% and ~36%, respectively. The porosity of the bulk of the wafer consisted of two parts: one associated with the finger-like macrovoids, called macroporosity, and the other associated with the small pores present in the solid phase and thus called microporosity. The macroporosity can be derived from the low magnification image, while the microporosity is determined from the high magnification image, focused on the solid phase of the bulk (the center) of the wafer. From Fig. 5F, the macroporosity was determined to be ~34%. From Fig. 5H, the percentage of pixels assigned to the small pores in the solid phase of the bulk (P_s) was determined to be ~36%. The volume fraction of this solid phase (V_s) was 66% of the whole wafer,

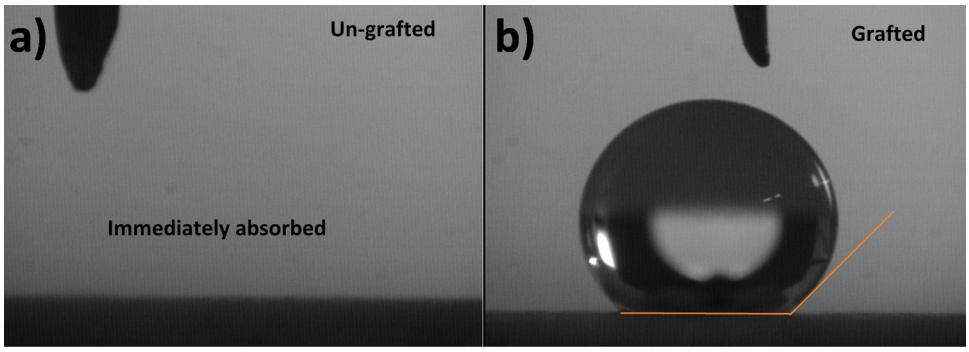

Fig. 8. Photographs of a water droplet on (A) un-grafted and (B) FAS-grafted alumina wafer, showing contact angles of 0° (absorbed) and 133°, respectively.

inferred from the macroporosity value (34%). Thus, the microporosity, the product of V_s and P_s, was calculated to be ~24% (36% × 66%). The sum of the macroporosity and microporosity was ~58% (34 + 24%), which was in good agreement with the porosity derived from the density data derived from Archimedes method.

3.4. Gas and liquid permeation

Fig. 7 shows the nitrogen and pure water flux as function of the trans membrane pressure of the alumina wafer. From these data a N_2 permeance of 1.1×10^6 L m^{-2} h^{-1} bar^{-1} and a pure water permeance of 9.4×10^3 L m^{-2} h^{-1} bar^{-1} was calculated. These values are much higher than porous multi-layer ceramics and comparable with that of hollow fibers prepared by the phase-inversion method.[22] As shown in the previous section, the wafer consisted of a relatively dense bottom layer that is expected to be less permeable to gases and liquids. This was confirmed by the large increase in permeability after mechanical removal of the bottom layer. The wafer without the bottom layer exhibited a N_2 permeance of 4.0×10^6 L m^{-2} h^{-1} bar^{-1} and a pure water permeance of 9.4×10^4 L m^{-2} h^{-1} bar^{-1}. The removal of the bottom layer led to an increase in gas permeance by a factor of nearly 3.5, and water permeance by an even larger factor of 10. The difference in the increase in permeance between gas and pure water could be attributed to their different transport mechanism. Clearly, the permeance of the bulk layer was much higher than that of the bottom layer, which is simply due to the existence of macrovoids in the bulk layer. These results indicate that the aligned finger-like pores are beneficial in reducing resistance and so the membranes will be suitable for membrane distillation application.

The wetting behavior of the membranes was evaluated by measuring the water contact angle. As can be seen from Fig. 8, water droplets were immediately absorbed when dripped onto the un-grafted membrane owning to the porosity and the naturally hydrophilic character of its surface. Values of the contact angle for the grafted membrane were in the range of 130–135° with an average of 133°, proving that the membrane surfaces were successfully changed into hydrophobic by grafting with FAS.

Fig. 9 shows the nitrogen and pure water fluxes of the un-grafted and grafted membrane. The nitrogen permeance was

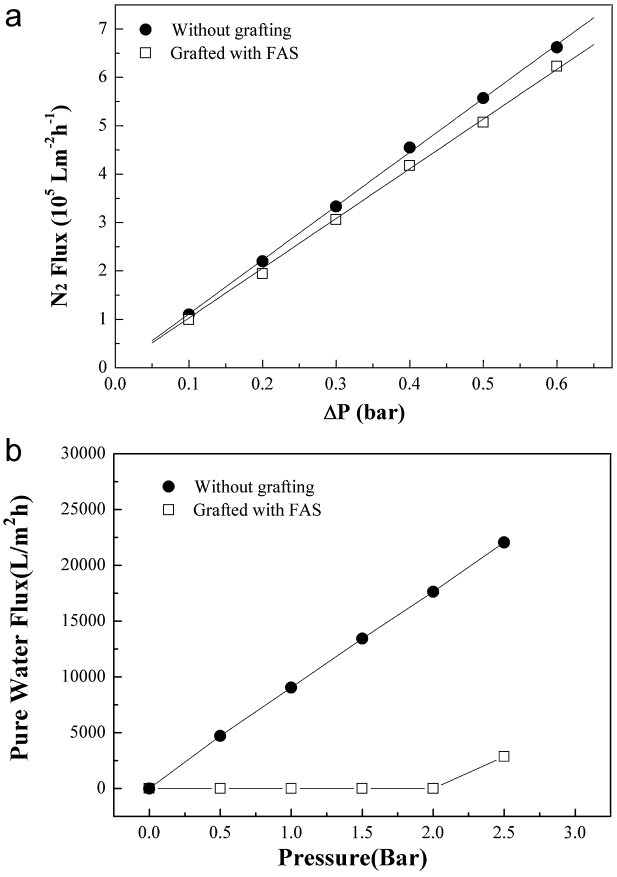

Fig. 9. (A) N_2 and (B) pure water flux of a ceramic wafer before and after FAS-grafting.

slightly decreased by 9% after grafting. The pure water permeance remained zero until a transmembrane pressure of 2 bar achieved. This value is called the liquid entry pressure (LEP), meaning that the grafted, hydrophobic membrane can operate under membrane distillation conditions at transmembrane pressures of up to 2 bar.

3.5. Water desalination performance

Direct contact membrane distillation performance of FAS-grafted porous alumina wafers was tested at several feed temperatures and varying NaCl concentrations.

Table 1
Comparison of the maximum flux obtained in this study with the literatures for DCMD process.

Membrane	Water flux (kg/m^2 h)	Feed side			Permeate side		Reference
		NaCl concentration	Inlet temp. (°C)	Fluid velocity	Inlet temp. (°C)	Fluid velocity	
PP hollow fiber	40.5	3.5 wt.%	82	0.50 m/s	20	0.15 m/s	23
PVDF flat sheet	18.9	35 g/L	73	54 L/h	25	54 L/h	24
PVDF flat sheet	32.4	Distilled	70	2.59 m/s	20	4.67 m/s	25
PVDF hollow fiber	21.2	3.5 wt.%	70	11.4 L/h	25	6 L/h	26
Al_2O_3 planar memb.	17.0	0.1 mol/L	53	–	17	–	27
Al_2O_3 planar memb.	6.8	0.1 mol/L	95	–	5	–	4
Si_3N_4 hollow fiber	12.5	2.0 wt.%	80	–	20	–	7
Al_2O_3 planar memb.	19.1	2.0 wt.%	80	0.03 m/s	20	0.03 m/s	This work

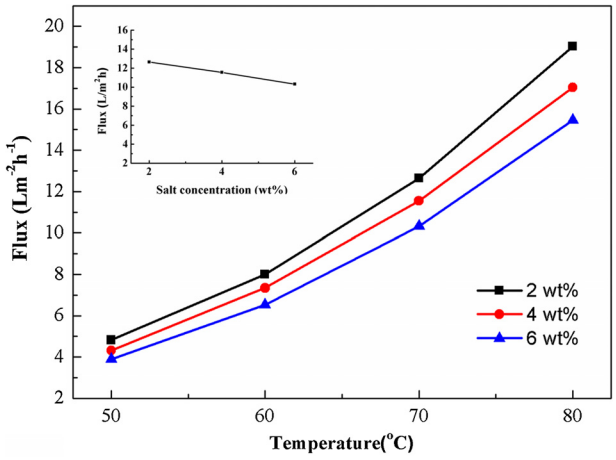

Fig. 10. Permeate Flux as a function of temperature in DCMD with various NaCl solutions (inset shows the flux as a function of NaCl concentration at 70 °C).

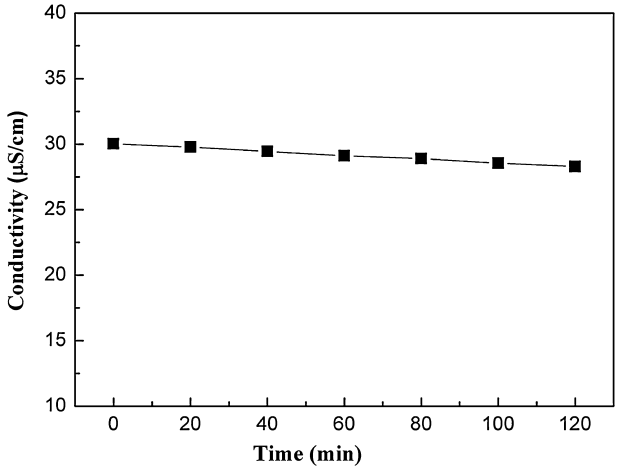

Fig. 11. Conductivity of the cold side water as a function of time (salt concentration of 2 wt.% and temperature of 80 °C for the feed solution).

Fig. 10 illustrates the flux as function of the feed temperature for various NaCl concentrations in DCMD. A significant increase in pure water flux is observed with increasing feed temperature. For example, a feed solution with a salt concentration of 2 wt.% shows an increase in water flux from 4.9 L m^{-2} h^{-1} to 19.1 L m^{-2} h^{-1} while the temperature increased from 50 °C to 80 °C. The driving force for desalination by means of membrane distillation is the difference in water vapor pressure between feed and permeate. A higher feed temperature results in a higher vapor pressure.

As shown in the inset of Fig. 10, the water flux decreased with increasing salt concentration at a fixed temperature. It is known from the Raoult's law that the water partial vapor pressure of a salt solution is equal to the vapor pressure of the pure water multiplied by the salt mole fraction. With increasing salt concentration, the water vapor pressure decreases. Nevertheless, even with a relatively high concentration of 6 wt.% NaCl, the water flux was still as high as 15.5 L m^{-2} h^{-1} at 80 °C.

Fig. 11 shows the electrical conductivity of the permeate side water. It can be seen that the water had a very small conductivity, indicating that the permeate side water was very pure and free of NaCl. The water at the permeate side was a mixture of water permeated from the feed side and the circulating cooling water (distilled water). It is observed that the conductivity decreased from 30.02 μS/cm to 27.62 μS/cm after 2 h. This reveals that the permeate water was purer than the cooling water, and the conductivity of the permeate water should be less than 27.62 μS/cm. Since the conductivity of feed salt water was 6.98 mS/cm, a high salt rejection over 99.5% was achieved after desalination. Meanwhile, the MD flux also showed no decline after 4 h desalination.

The fluxes obtained in this study are comparable with most of the polymer membranes and higher than the other ceramic membranes as shown in Table 1,[4,7,23–27] but it is still lower than the data of Hou and Phattaranawik,[23,25] which is likely due to the fact that the operation conditions in our case were not optimal. In particular, the flow rates at the feed and permeate side were much lower than those in their studies. It is well known that in membrane distillation temperature/concentration polarization results in a decreased driving force for transport and a lower mass flux. It has been shown that the polarization effects can be effectively diminished through increasing the flow rates.[28] Therefore, we expect that a higher flux can be obtained with our membranes when the flow rates are increased and other operation parameters are optimized.

4. Conclusions

Hydrophobic alumina planar membranes have been prepared using phase-inversion tape casting method as forming step, followed by sintering and subsequent grafting with a fluoroalkylsilane. The membrane exhibited a high porosity and

good gas/water permeance, owing to the very low resistance of the support layer and the uniform, small, pores of the separation layer. The FAS-grafted alumina membrane was successfully applied in the direct contact membrane desalination process. During the desalination of sodium chloride solution, the maximum water flux of 19.1 L m^{-2} h^{-1} with a 99.5% salt rejection was achieved. The ceramic planar membrane developed in this work is promising for practical applications.

Acknowledgements

This work was supported by National Natural Science Foundation of China (Grant No. 50972138) and Solar Energy Program of Chinese Academy of Sciences.

References

1. Zuo X, Peng C, Huang Q, Song S, Wang L, Li D, et al. Design of a carbon nanotube/magnetic nanoparticle-based peroxidase-like nanocomplex and its application for highly efficient catalytic oxidation of phenols. *Nano Res* 2009;**2**:617–23.
2. Song X, Liu Z, Sun DD. Nano gives the answer: breaking the bottleneck of internal concentration polarization with a nanofiber composite forward osmosis membrane for a high water production rate. *Adv Mater* 2011;**23**:3256–60.
3. El-Bourawi MS, Ding Z, Ma R, Khayet M. A framework for better understanding membrane distillation separation process. *J Membr Sci* 2006;**285**:4–29.
4. Larbot A, Gazagnes L, Krajewski S, Bukowska M, Kujawski W. Water desalination using ceramic membrane distillation. *Desalination* 2004;**168**:367–72.
5. Gazagnes L, Cerneaux S, Persin M, Prouzet E, Larbot A. Desalination of sodium chloride solutions and seawater with hydrophobic ceramic membranes. *Desalination* 2007;**217**:260–6.
6. Cerneaux S, Struzynska I, Kujawski WM, Persin M, Larbot A. Comparison of various membrane distillation methods for desalination using hydrophobic ceramic membranes. *J Membr Sci* 2009;**337**:55–60.
7. Zhang JW, Fang H, Wang JW, Hao LY, Xu X, Chen CS. Preparation and characterization of silicon nitride hollow fiber membranes for seawater desalination. *J Membr Sci* 2014;**450**:197–206.
8. Martinez-Diez L, Vazquez-Gonzalez MI. Temperature and concentration polarization in membrane distillation of aqueous salt solutions. *J Membr Sci* 1999;**156**:265–73.
9. Ahmad NA, Leo CP, Ahmad AL. Synthesis of superhydrophobic alumina membrane: effects of sol–gel coating, steam impingement and water treatment. *Appl Surf Sci* 2013;**284**:556–64.
10. Srisurichan S, Jiraratananon R, Fane AG. Mass transfer mechanisms and transport resistances in direct contact membrane distillation process. *J Membr Sci* 2006;**277**:186–94.
11. Vercauteren S, Keizer K, Vansant EF, Luyten J, Leysen R. Porous ceramic membranes: preparation, transport properties and applications. *J Porous Mater* 1998;**5**:241–58.
12. Verweij H. Ceramic membranes: morphology and transport. *J Mater Sci* 2003;**38**:4677–95.
13. He W, Huang H, Gao JF, Winnubst L, Chen CS. Phase-inversion tape casting and oxygen permeation properties of supported ceramic membranes. *J Membr Sci* 2014;**452**:294–9.
14. Fang H, Ren CL, Liu YG, Lu DT, Winnubst L, Chen CS. Phase-inversion tape casting and synchrotron-radiation computed tomography analysis of porous alumina. *J Eur Ceram Soc* 2013;**33**:2049–51.
15. Han XJ, Guan Y, Liu T, Tian YC, Chen CS. Determination of phase volume fractions of ceramic composite by synchrotron radiation computed tomography. *J Am Ceram Soc* 2012;**95**:2667–71.
16. Jakobs E, Koros WJ. Ceramic membrane characterization via the bubble point technique. *J Membr Sci* 1997;**124**:149–59.
17. Zhang JH, Dow N, Duke M, Ostarcevic E, Li JD, Gray S. Identification of material and physical features of membrane distillation membranes for high performance desalination. *J Membr Sci* 2010;**349**:295–303.
18. Luiten-Olieman MWJ, Raaijmakers MJT, Winnubst L, Bor TC, Wessling M, Nijmeijer A, et al. Towards a generic method for inorganic porous hollow fibers preparation with shrinkage-controlled small radial dimensions, applied to Al_2O_3, Ni, SiC, stainless steel, and YSZ. *J Membr Sci* 2012;**407**:155–63.
19. Li K, Tan XY, Liu YT. Single-step fabrication of ceramic hollow fibers for oxygen permeation. *J Membr Sci* 2006;**272**:1–5.
20. Otsu A. Threshoold selection method from gray-level histograms. *IEEE* 1979;**9**:62–6.
21. Yu J, Hu XJ, Huang Y. A modification of the bubble-point method to determine the pore-mouth size distribution of porous materials. *Sep Purif Technol* 2010;**70**:314–9.
22. Fang H, Gao JF, Wang HT, Chen CS. Hydrophobic porous alumina hollow fiber for water desalination via membrane distillation process. *J Membr Sci* 2012;**403**:41–6.
23. Hou DY, Wang J, Qu D, Luan ZK, Ren XJ. Fabrication and characterization of hydrophobic PVDF hollow fiber membranes for desalination through direct contact membrane distillation. *Sep Purif Technol* 2009;**69**:78–86.
24. Fan HW, Peng YL. Application of PVDF membranes in desalination and comparison of the VMD and DCMD processes. *Chem Eng Sci* 2012;**79**:94–102.
25. Phattaranawik J, Jiraratananon R, Fane AG. Heat transport and membrane distillation coefficients in direct contact membrane distillation. *J Membr Sci* 2003;**212**:177–93.
26. Drioli E, Ali A, Simone S, Macedonio F, Al-Jlil SA, Al Shabonah FS, et al. Novel PVDF hollow fiber membranes for vacuum and direct contact membrane distillation applications. *Sep Purif Technol* 2013;**115**:27–38.
27. Hendren ZD, Brant J, Wiesner MR. Surface modification of nanostructured ceramic membranes for direct contact membrane distillation. *J Membr Sci* 2009;**331**:1–10.
28. Schofield RW, Fane AG, Fell CJD, Macoun R. Factors affecting flux in membrane distillation. *Desalination* 1990;**77**:279–94.